Jarosław GUZIŃSKI[1], Haitham ABU-RUB[2], Patryk STRANKOWSKI[3]

Gdańsk University of Technology, Faculty of Electrical and Control Engineering (1,3),
Texas A&M University at Qatar, Faculty of Electrical and Computer Engineering (2)

Speed Sensorless AC Drive with Inverter LC Filter and Fault Detection Using Load Torque Signal

*Streszczenie. Wraz z rozwojem przemysłu nieustannie rośnie popularność silników indukcyjnych z uwagi na niskie koszty i dużą niezawodność. Aby spełnić takie wymagania przemysłu, prowadzi się intensywne badania w tej dziedzinie. Tej tendencji podporządkowuję się niniejszy artykuł, w którym pokazano rozwiązanie układu napędowego z silnikiem indukcyjnym, umożliwiające równoczesną detekcję uszkodzeń bez stosowania dodatkowych czujników, poza czujnikami standardowo stosowanymi w falownikach. Aby zrealizować taki układ napędowy z diagnostyką w czasie rzeczywistym zastosowano rozwiązanie z obserwatorem stanu do obliczania i analizy momentu elektromagnetycznego silnika. Zaproponowane rozwiązanie zastosowano do układu napędowego z filtrem sinusoidalnym, którego celem jest poprawa współczynnika THD napięcia zasilania silnika. Ponieważ filtr sinusoidalny komplikuje strukturę obserwatora stanu zastosowano rozszerzoną strukturę estymatora momentu silnika. Aby zbadać zaproponowane rozwiązanie wprowadzono sztuczne uszkodzenie polegające na niewyważeniu wirnika. Wyniki działania estymatora momentu porównano z wynikami pomiarów drgań przeprowadzonych przy użyciu akcelerometru. **Układ napędowy z silnikiem indukcyjnym, umożliwiający równoczesną detekcję uszkodzeń bez stosowania dodatkowych czujników**.*

Abstract. The industrial development in recent years has seen a major increase in the use of induction motors, whereby the cost has to be as low as possible and the lifetime as long as possible. To follow up this desire, investigations in this area have become very intense. For that reason, this paper presents a solution for driving an induction motor and simultaneous fault detection with no need for additional sensors. In order to achieve this target, an observer system is implemented and a torque estimation procedure is used for torque detection. An LC filter was installed at the inverter output to provide better THD of the current. The validation of the drive operation was achieved through simulation and experiments. To investigate possible faults, an artificial unbalance was introduced to the test bench, whereby the experiment was validated by a comparison of physical vibrations and estimated torque.

Słowa kluczowe: napęd bezczujnikowy, silnik indukcyjny, filtr sinusoidalny, detekcja uszkodzeń, obserwator momentu obciążenia
Keywords: sensorless drives, induction motor LC filter, fault detection, load torque observer, voltage converter

Introduction

Induction motor drives are widely used in industry because of their simple and robust design. To ensure their low cost operation over a long life span, in addition to increasing their reliability and efficiency, many research efforts have been dedicated to the monitoring and diagnostics of electric drives.

The demand for improving the efficiency, lifetime and condition of an electrical machine causes a rising interest in developing filter systems, which fulfill this desire [1, 2, 3].

Nevertheless, the fast development of voltage source inverters has made high speed and multiphase drives [4–8] possible, but also caused the problems of common mode voltage to increase. The consequences of common mode voltage are visible in the degradation of the insulation lifetime and the worn out bearings. In order to reduce this impact, a passive LC filter was implemented. The advantages, of course, are obvious; however, such a filter causes a voltage drop as well as a phase shift of the voltage and current, which makes the parameterization of the control unit more difficult [9]–[17].

An additional point that is imposed by the industrial restriction is the undesired application of sensors, because each added element means a higher price and greater vulnerability of the system. For this reason, interest in the problem of controlling a machine with fewer or without sensors is increasing [18]–[20]. The most popular method used to prevent and detect motor faults is the MCSA (Motor Current Signature Analysis) with mathematical techniques, e.g. Fourier [21],[22] and Wavelet [23],[24] transformations. By investigating the current or the resulting calculation with this variable, it is possible to diagnose the state of the machine. Following this idea, investigations of the air-gap magnetic flux density in the rotor were performed to provide an early fault diagnosis of broken rotor bars of squirrel cage motors [25].

It was shown that motor faults are mainly classified into four sections- bearings (≈41%), stator (≈37%), rotor (≈10%) and other (≈12%) faults [26], [27]. Inaccurate installation of the drive unit and faults caused by imprecise manufacturing processes may result in complete failure of the drive unit. An influence on this type of failure is exerted by unintentional vibrations. These disturbances have an impact on the torque of the machine and allow conclusions to be drawn about the condition of the machine.

By putting this idea into practice, this paper presents the structure of the sensorless induction motor drive, where signals and sensors of the voltage fed inverter will be exclusively used. An essential part of the proper drive operation is presented in section two, which describes the mathematical model of the system, where the filter model was taken into account to the motor model. The third section presents the control system with implementation of the multi scalar motor model. Section four, five and six present the proposed observer system with a precise torque observer, which enables a new possibility of fault detection in electrical drives with a noninvasive way. The initial functional tests of the proposed drive system were done through simulations, which are presented in section seven. Section eight presents the experimental investigations of the industry desired sensorless drive system with fault detection. The fault was introduced with an artificial unbalance of the rotor. To demonstrate the fault detection possibility accelerometers tests of the drive were compared with the estimated torque values in different drive operations.

Model of the system

The proposed control system consists of a voltage inverter, LC filter and IM – the general topology is presented in Fig. 1. The LC filter was designed according to [10], [15] to smooth motor supply motor voltage (THD$_U$<5%) (Fig. 2).
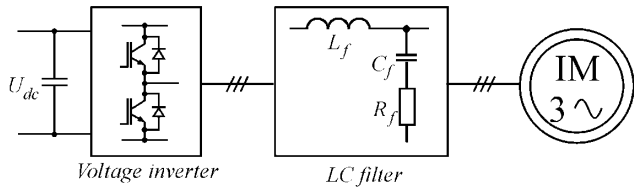
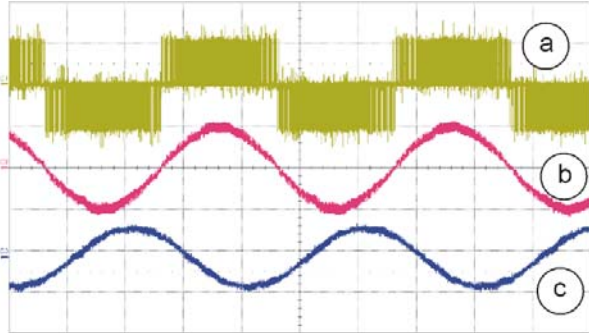Fig. 1. General topology of induction motor drive with inverter and LC filter

Fig. 2. Waveforms of the (a) inverter output voltage, (b) motor supply voltage (i.e. LC filter output voltage), and (c) motor current (respectively: 500 V/div, 200 V/div, 2 A/div, 10 ms/div)

The THD$_U$ is calculated as denoted in the next equation:

$$(1) \qquad THD = \left[\sqrt{\sum_{n=1}^{50} \frac{a_n^2}{a_1}} \cdot 100\% \right]$$

The model of the IM and LC filter is presented in a stationary reference frame noted as $\alpha\beta$. The inverse-Γ model (Fig. 3) of the IM was used due to reduction of unknown circuit parameters (ratio between stator and rotor self-inductances) [28], [29].
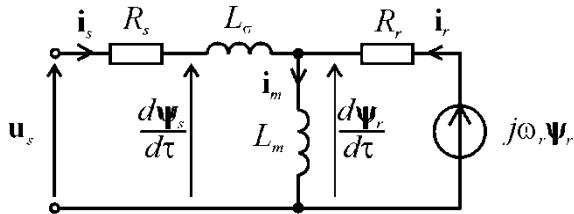

Fig. 3. Induction motor inverse-Γ equivalent circuit model

The IM model equations in per unit system [15] are:

$$(2) \quad \frac{d\mathbf{i}_s}{d\tau} = -\frac{R_s + R_r}{L_\sigma}\mathbf{i}_s + \frac{R_r}{L_m L_\sigma}\boldsymbol{\psi}_r - j\frac{1}{L_\sigma}\omega_r\boldsymbol{\psi}_r + \frac{1}{L_\sigma}\mathbf{u}_s$$

$$(3) \qquad \frac{d\boldsymbol{\psi}_r}{d\tau} = -\frac{R_r}{L_m}\boldsymbol{\psi}_r + j\omega_r\boldsymbol{\psi}_r + R_r\mathbf{i}_s$$

$$(4) \qquad \frac{d\omega_r}{d\tau} = \frac{1}{J_M}\left(Im\left|\boldsymbol{\psi}_r^* \mathbf{i}_s\right| - t_L \right)$$

$$(5) \quad \boldsymbol{\psi}_r = \begin{bmatrix}\psi_{r\alpha} & \psi_{r\beta}\end{bmatrix}^T, \ \mathbf{i}_s = \begin{bmatrix}i_{s\alpha} & i_{s\beta}\end{bmatrix}^T, \ \mathbf{u}_s = \begin{bmatrix}u_{s\alpha} & u_{s\beta}\end{bmatrix}^T$$

where $\mathbf{u}_s$, $\mathbf{i}_s$, $\boldsymbol{\psi}_r$ denote the stator voltage, stator current and rotor flux vectors, t_L − motor load torque, J_M − motor inertia and L_m, L_σ, R_s, R_r are the motor parameters [30].

The LC filter $\alpha\beta$ circuit is presented in Fig. 4, and the equations of model are [9]:

$$(6) \qquad \frac{d\mathbf{u}_c}{d\tau} = \frac{\mathbf{i}_c}{d\tau}C_f$$

$$(7) \qquad \frac{d\mathbf{i}_{inv}}{d\tau} = \frac{\mathbf{u}_{inv} - R_c\mathbf{i}_c - \mathbf{u}_c}{L_f}$$

$$(8) \qquad \mathbf{i}_c = \mathbf{i}_{inv} - \mathbf{i}_s$$

$$(9) \qquad \mathbf{u}_s = R_f\left(\mathbf{i}_{inv} - \mathbf{i}_s\right) + \mathbf{u}_c$$
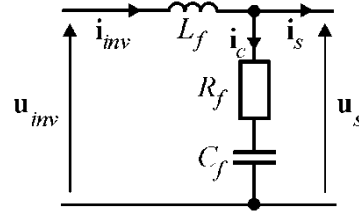

Fig. 4. LC filter $\alpha\beta$ equivalent circuit

Resistance of the L_f inductor is omitted. R_f is the damping resistor. The IM and LC filter parameters are given in Table I.

Control System

The control system consists of two parts, main and secondary. The main part is used for controlling the motor state variables, whereas the secondary (additional) part is used for LC filter control as shown in Fig. 5.

For the motor control, the nonlinear control principle was used. The used control algorithm idea was presented first time in [49] and named as multiscalar model based control (MMB). The MMB simple concept is to control only the selected natural variables as speed, torque and flux in the way to assure the system controllability in full operation range. The MMB method is simpler to implement than field oriented control (FOC) mainly due to elimination of Park transformation. The control properties of MMB are significantly better than FOC because of elimination model nonlinearities and cross-coupling between torque and flux regulation [15, 50]. That control idea is also known as natural variable model which is described in [31] in case of double fed induction machine. The natural variables are motor speed ω_r, torque Te and square of the magnitude of rotor flux linkage ψ_{rr}:

$$(10) \qquad T_e = \psi_{r\alpha}i_{s\beta} - \psi_{r\beta}i_{s\alpha}$$

$$(11) \qquad \psi_{rr} = \psi_{r\alpha}^2 + \psi_{r\beta}^2$$

As was presented in [15, 49, 50] to assure the full controllability of the motor it is necessarily simultaneously control the reactive torque T_r of the motor:

$$(12) \qquad T_r = \psi_{r\alpha}i_{s\alpha} + \psi_{r\beta}i_{s\beta}$$

With the set of variables (10)-(12) the IM multiscalar model is as follows:

$$(13) \qquad \frac{d\omega_r}{d\tau} = \frac{T_e}{J_M} - \frac{t_L}{J_M}$$

$$(14) \qquad \frac{dT_e}{d\tau} = -\frac{1}{T_v}T_e - \omega_r(T_r + \frac{1}{L_\sigma}\psi_{rr}) + \frac{1}{L_\sigma}u_1$$

$$(15) \qquad \frac{d\psi_{rr}}{d\tau} = -2\frac{R_r}{L_m}\psi_{rr} + 2R_rT_r$$

$$(16) \qquad \frac{dT_r}{d\tau} = -\frac{T_r}{T_v} + \omega_rT_e + \frac{R_r}{L_mL_\sigma}\psi_{rr} + R_r\frac{T_e^2 + T_r^2}{\psi_{rr}} + \frac{1}{L_\sigma}u_2$$
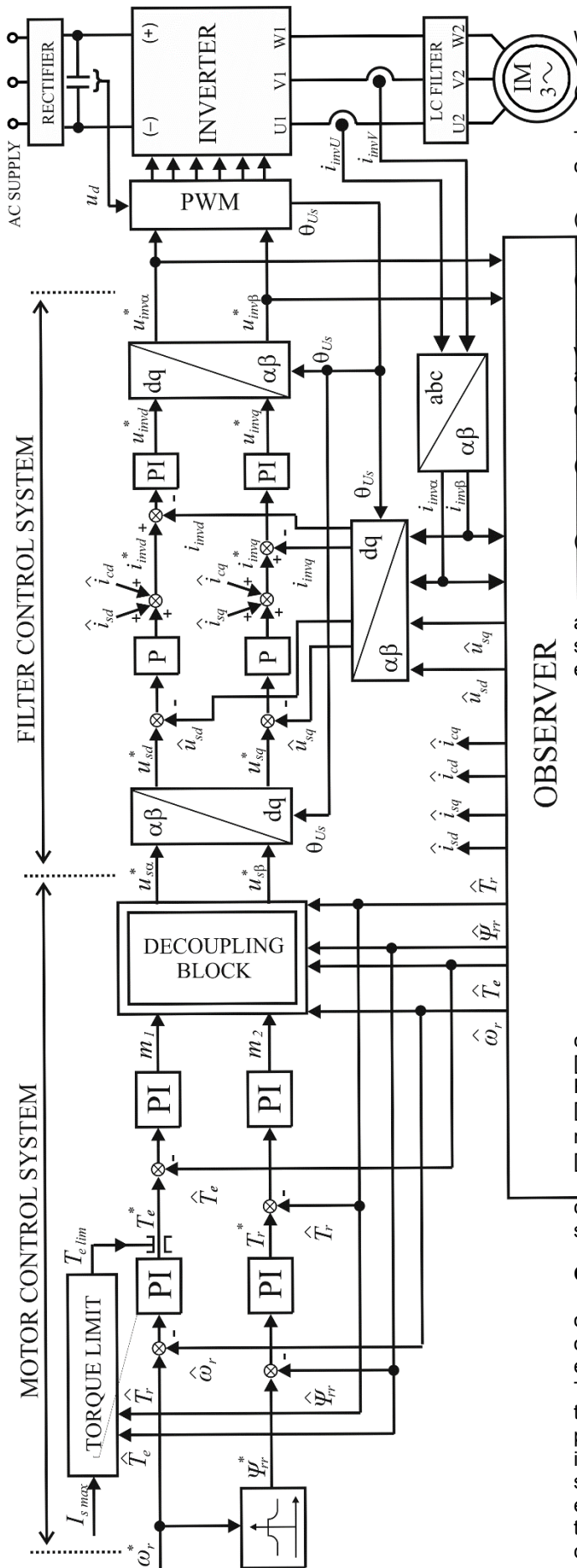
Fig. 5. Structure of the IM & LC filter sensorless control system

Where

$$(17) \qquad T_v = \frac{L_\sigma L_m}{R_r L_\sigma + L_m \left(R_s + R_r\right)}$$

The nonlinear parts appearing in (14) and (16) are compensated by control functions:

$$(18) \qquad u_1 = \omega_r \left(L_\sigma T_r + \psi_{rr}\right) + L_\sigma m_1$$

$$(19) \qquad u_2 = -L_\sigma \omega_r T_e - \frac{R_r}{L_m} \psi_{rr} - R_r L_\sigma \frac{T_e^2 + T_r^2}{\psi_{rr}} + L_\sigma m_2$$

where m_1, m_2 are the internal control signals, and u_1, u_2 are the auxiliary variables used for evaluating the motor commanded voltage $\mathbf{u}_s^*$:

$$(20) \qquad u_{s\alpha}^* = \frac{\psi_{r\alpha} u_2 - \psi_{r\beta} u_1}{\left|\mathbf{\psi}_r\right|^2}$$

$$(21) \qquad u_{s\beta}^* = \frac{\psi_{r\alpha} u_1 - \psi_{r\beta} u_2}{\left|\mathbf{\psi}_r\right|^2}$$

With (18)-(21), the induction motor model is decoupled and converted into adequate model which includes two separate linear subsystems: mechanical and electromagnetic [9], [32], [33]:

$$(22) \qquad \frac{d\omega_r}{d\tau} = \frac{T_e}{J_M} - \frac{t_L}{J_M}$$

$$(23) \qquad \frac{dT_e}{d\tau} = -\frac{1}{T_v} T_e + \frac{1}{L_\sigma} m_1$$

$$(24) \qquad \frac{d\psi_{rr}}{d\tau} = -2\frac{R_r}{L_m} \psi_{rr} + 2R_r T_r$$

$$(25) \qquad \frac{dT_r}{d\tau} = -\frac{1}{T_v} T_r + \frac{1}{L_\sigma} m_2$$

For the LC filter control an internal multi-loop feedback controller with disturbance compensation was used [11], [12]. It is a cascade structure with inner PI and outer P controller – the classical structure used for LC filters [15], [34]. The whole LC filter control is done in the rotating dq–reference frame aligned with the position of the $\mathbf{u}_s$ vector [9], [15].

As presented in Fig. 5, the motor control as well LC filter control is based on actual values estimated in the observer system.

Observer system

The essential part of the sensorless drive is the state observer which is based on the idea of the disturbance observer given in [33]. The observer has redundant equations used for disturbances (motor EMF) estimation. The accuracy of the estimation depends on the precision of the EMF model with restriction of some calculation problems in the case of the full EMF model. So in the implemented observer the component related to the motor speed derivative was omitted, assuming that for a small enough step of observer calculation this component is close to zero. With that, the numerical problems with derivative calculations were omitted. Additionally, the LC filter model (5)-(8) was included so the basic structure from [33] was extended to include a complex control object [13]–[15], [34],

[35]. Finally (contrary to [14]), in this paper the coefficients in the observer equations were simplified due to the concept of the inverse-Γ motor model instead of the previously used T model.

The complete structure of the observer is given by

$$(26) \quad \frac{d\hat{\mathbf{i}}_s}{d\tau} = -\frac{R_s + R_r}{L_\sigma}\hat{\mathbf{i}}_s + \frac{R_r}{L_m L_\sigma}\hat{\boldsymbol{\psi}}_r - j\frac{1}{L_\sigma}\hat{\boldsymbol{\xi}} + \frac{1}{L_\sigma}\mathbf{u}_s + k_1\left(\mathbf{i}_{inv} - \hat{\mathbf{i}}_{inv}\right)$$

$$(27) \quad \frac{d\hat{\boldsymbol{\psi}}_r}{d\tau} = -\frac{R_r}{L_m}\hat{\boldsymbol{\psi}}_r + j\hat{\boldsymbol{\xi}} + R_r\hat{\mathbf{i}}_s + \mathbf{e}_\psi$$

$$(28) \quad \frac{d\hat{\boldsymbol{\xi}}}{d\tau} = -\frac{R_r}{L_m}\hat{\boldsymbol{\xi}} + R_r\hat{\omega}_r\hat{\mathbf{i}}_s + j\hat{\omega}_r\hat{\boldsymbol{\xi}} + jk_4\left(\mathbf{i}_{inv} - \hat{\mathbf{i}}_{inv}\right)$$

$$(29) \quad \frac{dS_{bF}}{d\tau} = k_{fo}\left(S_b - S_{bF}\right)$$

$$(30) \quad \frac{d\hat{\mathbf{u}}_c}{d\tau} = \frac{1}{C_f}\left(\mathbf{i}_{inv} - \hat{\mathbf{i}}_s\right)$$

$$(31) \quad \frac{d\hat{\mathbf{i}}_{inv}}{d\tau} = \frac{1}{L_f}\left(\mathbf{u}_{inv}^* - \hat{\mathbf{u}}_s\right) + k_A\left(\mathbf{i}_{inv} - \hat{\mathbf{i}}_{inv}\right) + jk_B\left(\mathbf{i}_{inv} - \hat{\mathbf{i}}_{inv}\right)$$

$$(32) \quad \hat{\mathbf{u}}_s = \hat{\mathbf{u}}_c + \left(\mathbf{i}_{inv} - \hat{\mathbf{i}}_s\right)R_f$$

$$(33) \quad \mathbf{e}_\psi = \begin{bmatrix} -k_2 S_b \hat{\psi}_{r\alpha} + k_3 \hat{\psi}_{r\beta}\left(S_b - S_{bF}\right) \\ -k_2 S_b \hat{\psi}_{r\beta} - k_3 \hat{\psi}_{r\alpha}\left(S_b - S_{bF}\right) \end{bmatrix}$$

$$(34) \quad \hat{\boldsymbol{\xi}} = \hat{\omega}_r \boldsymbol{\psi}_r$$

where: $\boldsymbol{\xi}$ is the motor electromotive force (EMF), k_1, k_2, k_3, k_4, k_A, k_B are the observer gains, S_b is the observer internal stabilizing component, S_{bF} is the filtered value of S_b, and k_{fo} is the inverse of filter time constant.

The motor speed is estimated as follows:

$$(35) \quad \hat{\omega}_r = \frac{\hat{\xi}_\alpha \hat{\psi}_{r\alpha} + \hat{\xi}_\beta \hat{\psi}_{r\beta}}{\hat{\psi}_{rr}}$$

The only possibility for sensorless drive (no sensors used on the filter output) is that the observer feedback has to be a difference between the measured and estimated inverter output current – eq. (26), (28) and (31). Further details on initial observer system theory, tuning and stability, were presented without the LC filter in [33] and with the filter in [9], whereas for the complex observer (e.g. motor & LC filter) details are given in [15]. This paper uses the same structure as presented earlier in [15] but with a different coefficient appearing in the observer equations. The difference arises from the use of the inverse-Γ motor model, where total leakage inductance appears instead of separate leakage inductances for stator and motor.

Load Torque Estimation

The load torque signal could be used for diagnostic purposes [30], [36]–[40]. Frequency analysis of this signal leads to the possibility of detecting natural frequencies related to different fault types of the mechanical system. Widely used methods are based on the measurements using accelerometers [10], [41]–[43]. Measurement based methods are not practical for industrial applications. Therefore, there is a demand for seeking sensorless solutions based on a computation of motor torque using easily measured signals such as current, voltage or speed [44]–[47].

In this solution, the load torque observer used is based on Gopinath's theory [37], [48]:

$$(36) \quad \frac{d\mathbf{z}}{dt} = \begin{bmatrix} 0 & -k_{1L} \\ 1 & -k_{2L} \end{bmatrix}\mathbf{z} + \begin{bmatrix} k_{1L}k_{2L}J_M \\ \left(k_{2L}^2 - k_{1L}\right)J_M \end{bmatrix}\hat{\omega}_r + \begin{bmatrix} k_{1L} \\ k_{2L} \end{bmatrix}\hat{T}_e$$

$$(37) \quad \hat{T}_L = z_2 - k_{2L}J_M\hat{\omega}_r$$

where: $\hat{T}_L$ is the estimated motor load torque, $\mathbf{z} = \begin{bmatrix} z_1 & z_2 \end{bmatrix}^T$ is the load torque observer internal state variable, $\hat{T}_e$ is the calculated motor electromagnetic torque, k_{1L}, k_{2L} are the observer coefficients, and $\hat{\omega}_r$ is an estimated speed – eq. (35).

Based on speed observer (26)-(35) estimated flux and current the motor electromagnetic torque is calculated as follows:

$$(38) \quad \hat{T}_e = \psi_{r\alpha}\hat{i}_{s\beta} - \psi_{r\beta}\hat{i}_{s\alpha}$$

The solution presented in this paper was implemented in earlier authors' works for high speed train traction drives without LC filters [30] and for sensorless drive with filter [14]. In this paper the load torque observer has a simpler construction due to the inverse-Γ motor model used. Fig. 6 presents the structure of the applied load torque observer structure.
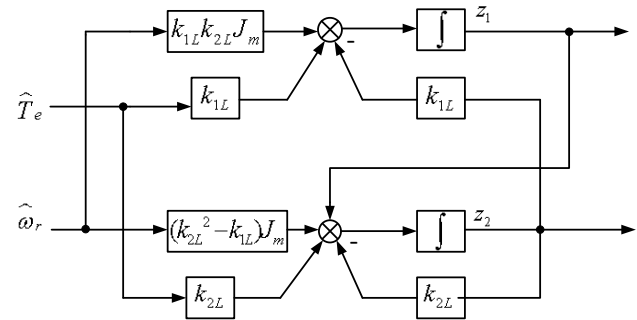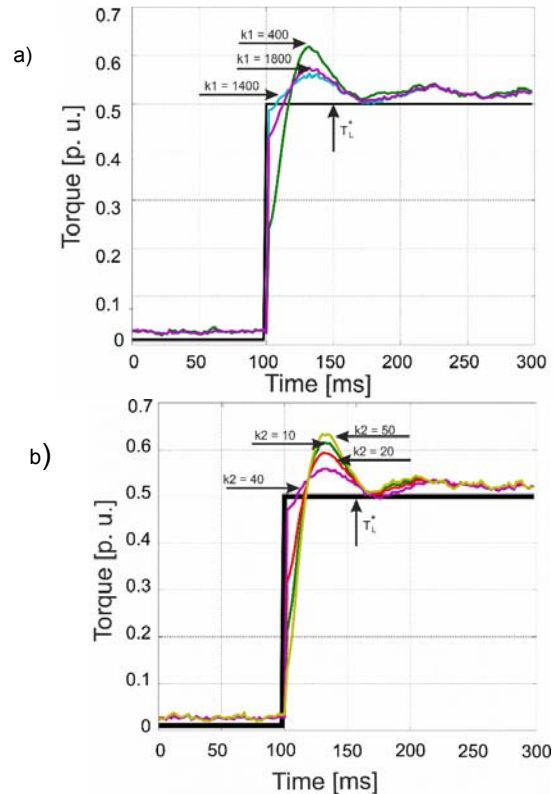

Fig. 6 Structure of the applied observer.

Fig. 7 Empirical observer coefficient selection: a) k_{2L} was constant, where k_{1L} was varied, b) k_{1L} was constant and k_{2L} was changed

The essential task for an accurate observer operation is to choose the right observer coefficients k_{1L} and k_{2L}. A less complicated way to choose these factors is given through empirical experiments in the simulations. Fig.7 shows the behavior of the estimated load torque T_L of the observer compared to the desired load torque T_L^* of the key values. In the first experiment (Fig. 7 a)) the coefficient k_{2L} was constant to see the influence on the changed coefficient k_{1L}. In contrast to the first test, the second test (Fig. 7 b)) was done with a constant k_{1L} and a varied k_{2L}. As can be seen in Fig.7, the best values are located inside the boundaries that have to be found with numerous tests. The two best coefficients $k_{1L} = 1400$ and $k_{2L} = 40$ were chosen for the real experiment.

Fault identification

As mentioned in the introduction, a good way to investigate fault symptoms of a drive system is the Fast Fourier Transformation (FFT), which offers an insight into the frequency components of the analyzed signal. The necessary harmonics that identify the fault symptoms were concluded from numerous comparisons of healthy and disturbed motor drives as presented in section eight. The equation (40) describes the relation of the frequencies that indicate a fault in the induction machine:

$$(39) \quad f_{fault} = \frac{s}{p} \cdot f_s \cdot k$$

where f_{fault} is the frequency that indicates a fault, s is the slip of the induction motor, f_s is the stator frequency and $k = 1,2,3,...$ is the factor of the searched harmonics.

This knowledge makes it possible to realize an online fault detection in a relatively less complicated way and furthermore with less computing power than in other applications, as presented in [28], [29]. Fig. 8 shows a possible method to implement online fault detection or online fault monitoring.
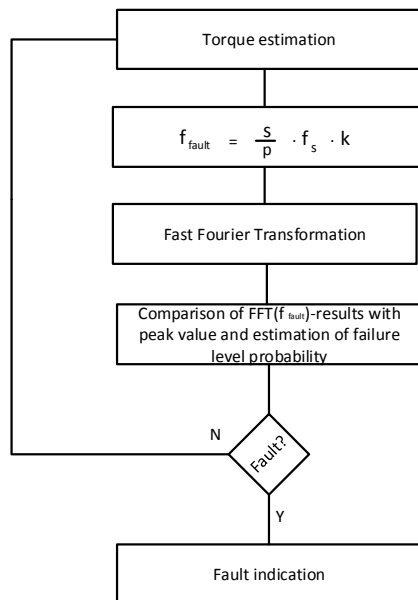

Fig. 8. Algorithm of online fault monitoring

The torque that is simultaneously estimated can be used in connection with an FFT analysis to observe the relevant frequencies as described in equation (40). A peak value that is based on the empirical values for the drive system serves as a comparative tool to identify a possible failure. In connection with a modern digital signal processor, which offers a relatively high computing power, the fault detection algorithm can be implemented without any technical expense or effort.

Simulation Investigations

At first simulation results of IM drive with LC filter were done to confirm the speed sensorless operation. Selected representative results are shown in Fig. 9.
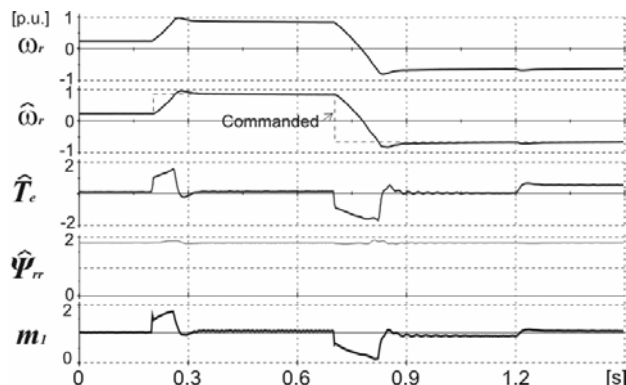

Fig. 9. Simulation results of the sensorless control system during speed and load variations.

Fig. 9 shows the reference speed changes, including motor reverse, as well load torque change at constant speed. The drive operates as required. The rotor flux variable (Ψ_{rr}) is kept constant except for the small oscillations in transients which are the result of the controllers' output saturation. It is noticeable that the motor torque T_e is limited during transients. This arises from the imposed condition used to keep the motor current within the safe limit,

$$(40) \quad T_{e\,lim} = \sqrt{I_{s\,max}^2 \cdot \hat{T}_e - \hat{T}_r^2}$$

where $T_{e\,lim}$ is the output limit of the speed controller as shown in Fig. 10, and $I_{s\,max}$ is the safe maximum of the motor current. That condition is required in the proposed control structure (because stator current is not directly controlled) to protect the motor against overload.
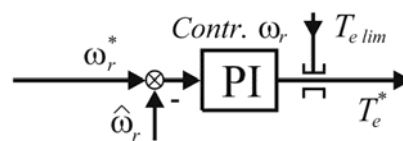

Fig. 10. Limiter of the maximum allowed torque for motor current protection.

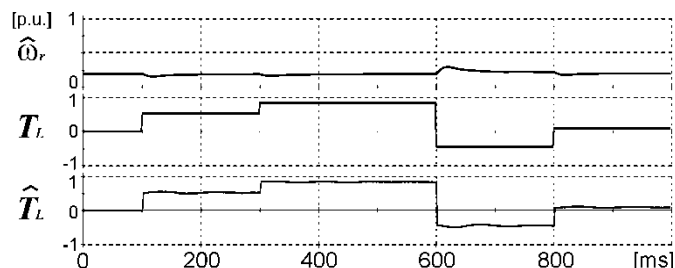An example of the load torque observer results is presented in Fig. 11.

Fig. 11. Simulation results of the load torque observer – comparison of the real load torque T_L with estimated torque $\hat{T}_L$.

In Fig. 11, the motor load torque step change was applied, while the motor commanded speed was kept constant. The estimated load torque $\hat{T}_L$ is very close to the real torque T_L. The highest error does not exceed 5% in transients when large load torque is applied. The nominal motor torque is ca. 0.65 p.u..

Experimental investigations

The investigations were done on the laboratory test bench with a 1.5 kW induction motor coupled with a dc generator. Both machines were connected to converters: an IGBT inverter and a thyristor based DC current controller. To obtain smooth motor stator voltage, a low pass filter was installed on the inverter output. The filter was designed to keep the motor voltage THD_U less than 5%, with restriction of the motor supply voltage drop up to 4% of the rated one. The sensors required for closed loop drive operation are dc link voltage and two current sensors at the inverter output. The speed sensor was installed only for data acquisition and is not needed for drive operation. Furthermore, to investigate the vibrations of the system, two accelerometers were installed at the motor frame and test bench base. The whole machine systems were installed on vibroisolators. To prevent the gearing current two common mode (CM) chokes were installed. A schematic representation of the test bench is shown in Fig. 12, while the system data are given in Table 1.
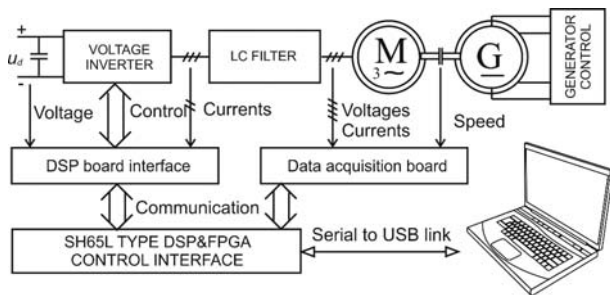

Fig. 12. Structure of the test bench - IM drive with inverter, LC filter and control system
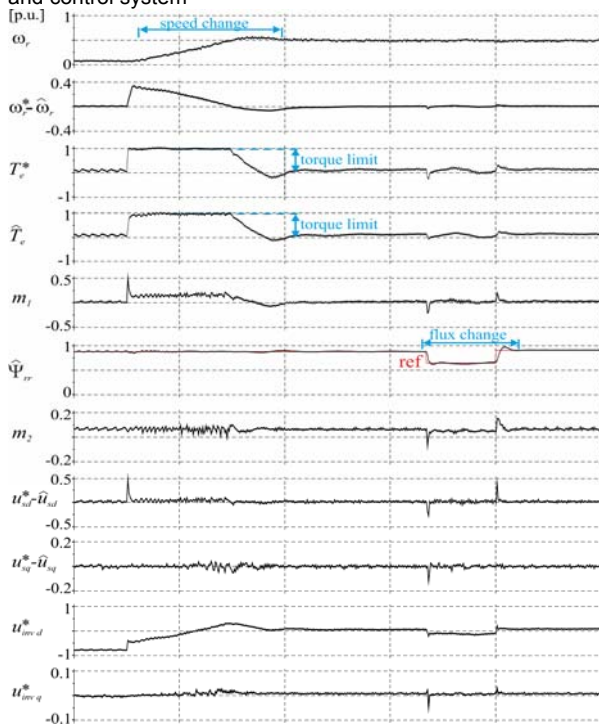

Fig. 13. Experimental results of speed sensorless operation for speed and flux changes.

In order to ensure correct functioning of the sensorless control, a speed change test was done, as presented in Fig. 13. The measured and the estimated signals are shown for comparison purposes. The estimated speed is calculated only by the measured dc link voltage and the current measured at the input of the LC filter. The complete system works correctly, as can be seen from Fig. 13. More results of the sensorless system were presented in [13], [14],[39],[40].

To analyze the disturbed operation of the drive system, a fault motor state and artificial unbalance were installed on the anti drive side of the motor shaft, as illustrated in Fig. 14.

Furthermore, to refer to the physical values of the artificial generated vibrations, two accelerators were installed on the stator housing and test bench bar (for coincidence purposes). The load machine was used to simulate a stress state on the induction motor and to investigate the influence on the vibrations of this stress.
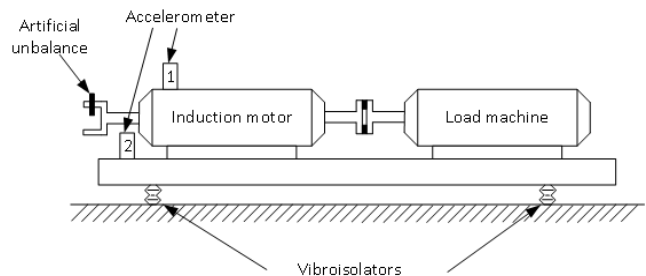

Fig. 14.Schematic representation of the investigated test bench

Table 1 –Data of the test bench

Asynchronous motor	
Power P_n	1.5 kW
Volatge U_n	300 V
Current I_n	4.7 A
Speed n_n	1420 rpm
Frequency f_n	50 Hz
Inertia J_M	0.0038 kg·m²
Stator resistance R_s	3.16 Ω
Rotor resistance R_r	2.31 Ω
Leakage inductance $L\sigma$	17 mH
Mutual inductance L_m	0.1779 H
Voltage inverter	
Switching frequency	3.3 kHz
Dead time	4.5 µs (compensated)
Pulse width modulation	Space vector
LC filter	
Inductance L_f	5.6 mH
Resistance R_f	0.05 Ω
Capacitance C_f	3 µF
Resistance R_c	1 Ω
Voltage drop ΔU	4.8 %
Voltage THD	≤5 %
Resonance frequency	1.2 kHz
Control system	
Calculation sampling	150µs (synchronized with PWM)
DSP program calc. time	80 µs
Vibration measurement	
Type of accelerometer	Piezoelectric
Measurement range	± 490 m/s²
Frequency range	0.5 Hz to 10 kHz
Resonant frequency	25 kHz

To demonstrate a fault detection, in the desired industrial solution with no additional sensors, the estimated torque from the observer was investigated in regard to the occurring motor fault state. The measured signal of the vibrations and equally the calculated torque from the observer were analyzed using the Fast Fourier Transform

(FFT). Because the primary upcoming frequency was in the range of 1 Hz–130 Hz, all frequency representations were scaled in to this range. The dc component of each FFT was removed. For a better comparison and for finding relations between different motor speeds, the figures are presented in a 3D-perspective.

Fig. 15 and 16 present the measured vibrations of the drive system without load. The peaks of the accelerations can be found at the rotor (f_r) and stator (f_s) frequency. Because of the number of poles $p=2$, the rotor rotating frequency is half of the electrical stator frequency and had the major influence on the vibrations. Furthermore harmonics such as $2f_s$ and the addition of rotor and stator frequency f_s+f_r can be found. The accelerations of the healthy drive system are relatively low, at about 3 m/s² compared to the maximum peak of the fault drive system at about 60 m/s2. It can be said that the magnitudes of the vibrations were, as supposed, rising with rising speed. The disturbed drive system (Fig. 16) shows a highly increased magnitude of acceleration in the vibrations. Contrary to expectations, the accelerations of the system did not increase with increasing rotor speed. The peak value of vibrations is at a rotor frequency of 25 Hz and could be explained by the installed vibroisolators, which come into resonance in this frequency range.
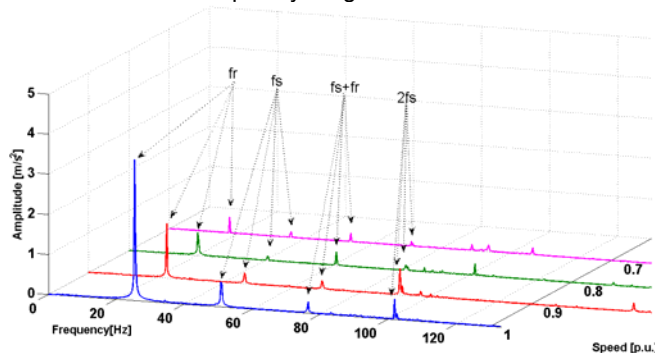

Fig. 15 FFT analysis of the measured vibrations (sensor 1) of healthy drive system without load.
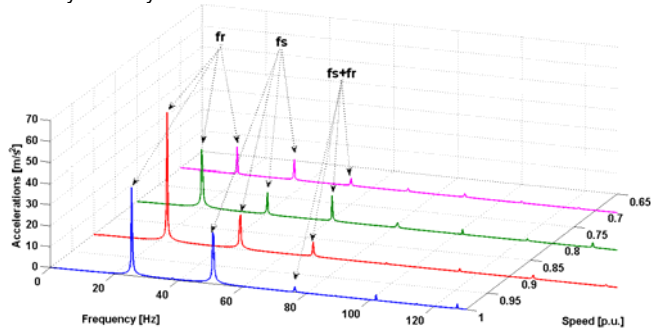

Fig. 16. FFT analysis of the measured vibrations (sensor 1) of the drive system with artificial unbalance and without load.
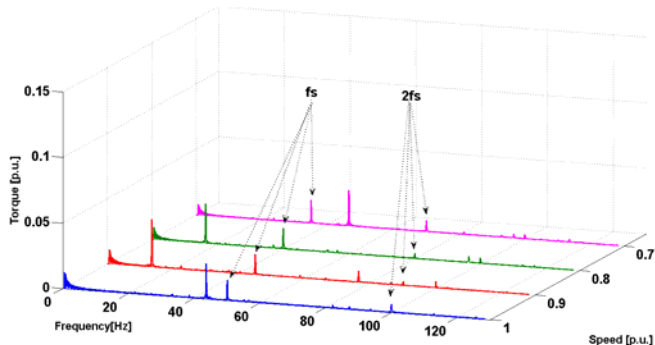

Fig. 17. FFT analysis of the estimated torque of the observer of a healthy drive system.

The previous evaluation of the experiment gives a reference value to the following experiment. To determine such a fault in the drive system, the industry desires a solution with no additional components. The estimated torque will be analyzed to avoid using additional sensors. Fig. 17 shows the FFT of calculated observer torque for the healthy drive system.

The peak of the stator frequency can be recognized in each speed state. This confirms that the drive system was free of any fault symptoms. The peaks are accurate and reproducible, but other peaks that can be seen are not reproducible and can be declared as noise or disturbance of the observer. The next illustration (Fig. 18) presents the estimated torque of the observer with artificial unbalance without load. Equally to the vibrations, the highest amplitude can be found at the rotor frequency f_r. These measurements verify the fault state of the drive system.
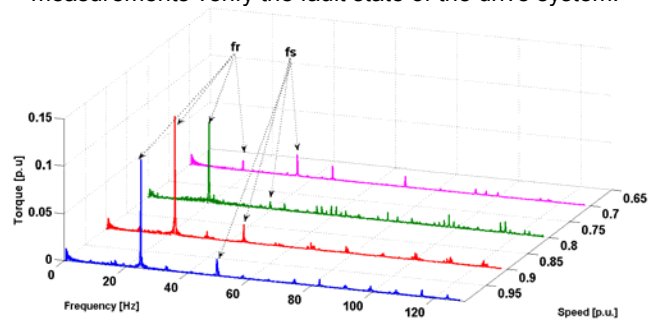

Fig. 18. FFT analysis of the estimated torque of the observer of the drive system with artificial unbalance – faulty drive.

The illustrations in Fig. 19 and Fig. 20 present the vibrations and the estimated torques of the drive system with artificial unbalance and loaded by the dc generator driven. The operating point of the motor In would be described as a load of 100%. Fig. 19 shows that the operation is very close to the measurements of Fig. 16. Nevertheless, the load causes an attenuation in the acceleration of the vibrations and a decreasing of the rotor speed. The calculated torque of the observer shows correspondingly an attenuation behavior close to the measured vibrations. This comparison demonstrates that the estimated torque is a variable, which can be reliably evaluated to detect faults in an electrical machine.
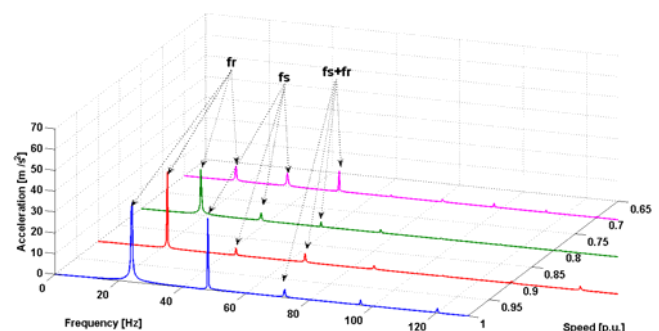

Fig. 19. FFT analysis of vibrations (sensor 1) of the drive system with artificial unbalance and loaded with 100%

As a further way to prove the assumption of sensorless fault detection and moreover to investigate the impact of different observers, another observer (observer 2) was implemented. In contrast to the first observer, the filter equations in the second observer are excluded. The experiment was done by moving the measurement points (current and voltage of the inverter) directly to the induction motor.
Fig. 21 and Fig. 22 present the results of the estimated torque of an observer excluding the LC filter.
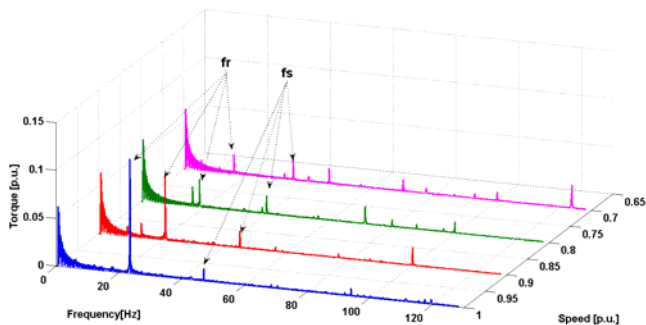
Fig. 20. FFT analysis of the estimated torque of the drive system with artificial unbalance and loaded with 100%.
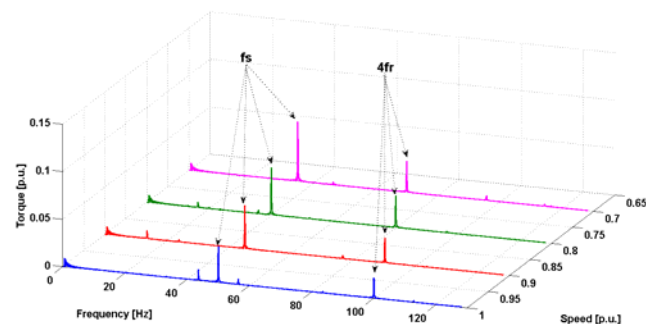

Fig. 21. FFT analysis of the estimated torque of the healthy drive system with observer 2

As shown in Fig. 21, the behavior of the frequency analysis is comparable with the results of the first observer. The rotor frequencies f_r are not present in the healthy condition, but the stator frequencies f_s result in other amplitudes. Nevertheless a further harmonic $4 \cdot f_r$ appears in the FFT analysis and noises are damped. In conclusion, as suggested, the change of the observer causes another outcomes of the analysis.
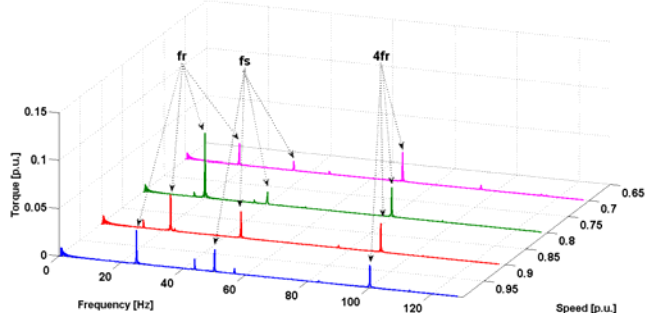

Fig. 22. FFT analysis of the estimated torque of the drive system with artificial unbalance and observer 2

Fig. 22 shows the FFT analysis of the disturbed drive system with the second observer. It is clearly noticeable that the rotor frequencies f_r appear, corresponding to the previous tests. The resonant frequency in this test is at the speed of $0.8 \cdot f_s$, which could be explained by a moved position of the drive system. However, this demonstrates that a disturbed operation of the drive system can be recognized by analyzing the estimated torque. Moreover, this illustrates that the parameterization and creation of the observer have an influence on the behavior of the analysis, while also allowing correct interpretation of a fault in the drive system.

Conclusion

The presented induction motor drive with voltage source inverter works properly at different operating points. Although an LC filter was used at the inverter output, it is possible to perform speed control over a wide range. A corrective action of the drive was possible after including a model of the LC filter in the observer structure and modeling control scheme.

The proposed idea of fault detection in the desired industry solution, with no additional sensors, detects load torque oscillations, which are caused by different defects in the mechanical load of the motor drive. Based on this, a sensor saving would result in an improvement of the economy and reliability of the complete drive system.

Furthermore the analysis of the load torque opens a further way to diagnose the condition of the mechanical drive part. The use of this additional component can improve the precision of fault detection or offer a further method for monitoring drive systems.

Autors: D. Sc. Jarosław Guziński, M.Eng Patryk Strankowski Gdańsk University of Technology, Department of Electrical and Control Engineering , ul. Narutowicza 11/12,80-233 Gdańsk Poland,E-mail:jaroslaw.guzinski@pg.gda.pl, patryk.strankowski@pg.gda.pl, strankowski.p@gmail.com; Prof. Dr. Haitham Abu-Rub Faculty of Electrical and Computer Engineering Texas A&M Engineering Building, Education City PO Box 23874 Doha Qatar E-Mail: haitham.abu-rub@qatar.tamu.edu

REFERENCES
[1]   M. Asadi, A. Jalilian Using an active resistive damper in hybrid active power filter to avoid resonance over-voltage, Electrical Engineering 95 (2013) pp. 301–313
[2]   Guzinski J., Abu-Rub H., Toliyat H.A.(2010) Speed sensorless ac drive with inverter output filter and fault detection using load torque signal, IEEE International Symposium on Industrial Electronics ISIE 2010, 4-7 July 2010, Bari, Italy, pp. 3113 - 3118
[3]   Stec P., Guzinski J., Strankowski P., Iqbal A. Abduallah Ahmad Anad, Abu-Rub H.: Five-Phase Induction Motor Drive with Sine-Wave Filter, IEEE International Symposium on Industrial Electronics ISIE 2014, Istanbul, Turkey, pp. 2111 – 2116
[4]   Arkadiusz Lewicki, Jarosław Guziński, Patryk Strankowski „Metoda wektorowej modulacji szerokości impulsów pięciofazowego falownika napięcia", Przegląd Elektrotechniczny, 05/ 2016
[5]   Marek Adamowicz, Patryk Strankowski, Jarosław Guziński, Zbigniew Krzemiński „Sterowanie multiskalarne pięciofazową maszyną indukcyjną", Przegląd Elektrotechniczny, 05/2016
[6]   Arkadiusz Lewicki, Jarosław Guziński, Patryk Strankowski „Wektorowa modulacja szerokości impulsów w pięciofazowych falownikach napięcia", XII Konferencja Naukowa Sterowanie w Energoelektronice i Napędzie Elektrycznym SENE 2015
[7]   Marek Adamowicz, Patryk Strankowski, Jarosław Guziński, Zbigniew Krzemiński „Sterowanie multiskalarne pięciofazowym silnikiem indukcyjnym" XII Konferencja Naukowa Sterowanie w Energoelektronice i Napędzie Elektrycznym SENE 2015
[8]   Levi E., Multiphase Electric Machines for Variable-Speed Applications, IEEE Trans. Ind. Electron., 55 (2008), n.5, 1893-1909
[9]   J. Guzinski Sensorless AC drive control with LC filter, in Proc. 13th European Conference on Power Electronics and Applications, EPE 2009. 8-10 September. Barcelona, Spain pp. 1 – 10
[10] Z. Krzemiński, J. Guziński Output filter for voltage source inverter supplying induction motor, Int. Conf. on Power Electronics, Intelligent Motions and Power Quality, PCIM 2005, Nuremberg, Germany
[11] J.Guziński, H. Abu-Rub, P.Strankowski Variable AC Drives with Inverter Output Filter (2015) John Wiley & Sons
[12] R. Seliga, W. Koczara Instantaneous current and voltage control strategy in low-pass filter based sine-wave voltage dc/ac converter topology for adjustable speed PWM drive system, IEEE

International Symposium on Industrial Electronics ISIE (2002),L'Aquila, Italy, pp. 813 - 817

[13] J. Guzinski, H. Abu-Rub Asynchronous motor nonlinear control with inverter output LC filter, 2nd Mediterranean Conference on Intelligent Systems and Automation (2009), Zarzis, Tunisia

[14] J. Guzinski, H. Abu-Rub, H.A. Toliyat Speed sensorless ac drive with inverter output filter and fault detection using load torque signal, IEEE International Symposium on Industrial Electronics ISIE 2010, 4-7 JulyBari, Italy, pp. 3113 - 3118

[15] H. Abu-Rub, A. Iqbal, J. Guzinski High Performance Control of AC Drives with Matlab / Simulink Models, (2012) John Wiley & Sons,.

[16] J. Salomaki, M. Hinkkanen, J. Luomi Sensorless control of induction motor drives equipped with inverter output filter, IEEE Transactions on Industrial Electronics, vol. 53, (2006) no. 4,, pp. 1188-1197.

[17] T. Tarczewski, L.M. Grzesiak PMSM fed by 3-level NPC sinusoidal inverter with discrete state feedback controller, 15th European Conference on Power Electronics and Applications EPE 2013, , Lille, France, pp. 1-9.

[18] V. Verma, C. Chakraborty, S. Maiti, Y. Hori Speed Sensorless Vector Controlled Induction Motor Drive Using Single Current Sensor, IEEE Transactions on Energy Conversion, vol. 28, (2013) no. 4, pp. 938 - 950

[19] G.D. Marques, D.M SousaNew Sensorless Rotor Position Estimator of a DFIG Based on Torque Calculations—Stability Study, IEEE Transactions on Energy Conversion, vol. 27 (2012), no. 1, pp. 196 - 203

[20] Matteo Felice Iacchetti,M. S. Carmeli ,Francesco Castelli Dezza R. Perini A speed sensorless control based on a MRAS applied to a double fed induction machine drive Electrical Engineering (2010) 95:301–313

[21] M. Pineda-Sanchez, M. Riera-Guasp J.A Antonino-Daviu, J. Roger-Folch, J. Perez-Cruz, R. Puche-Panadero, Diagnosis of Induction Motor Faults in the Fractional Fourier Domain, IEEE Transactions on Instrumentation and Measurement, vol. 59, no. 8 (2010), pp. 2065 - 2075

[22] J.H. Jung, J.J. Lee, B.-H. Kwon Online Diagnosis of Induction Motors Using MCSA, IEEE Transactions on Industrial Electronics, vol. 53, no. 6 (2006), 1842 - 1852

[23] A. Bouzida, O. Touhami, R. Ibtiouen, A. Belouchrani, M. Fadel, A. Rezzoug Fault Diagnosis in Industrial Induction Machines Through Discrete Wavelet Transform, IEEE Transactions on Industrial Electronics, vol. 58, no. 9, (2011) pp. 4385 - 4395

[24] E.C.C. Lau, H.W. Ngan Detection of Motor Bearing Outer Raceway Defect by Wavelet Packet Transformed Motor Current Signature Analysis, IEEE Transactions on Instrumentation and Measurement, vol. 59, no. 10 (2010), pp. 2683 - 2690

[25] K.N. Gyftakis, D.V. Spyropoulos, J.C. Kappatou, E.D. Mitronikas A Novel Approach for Broken Bar Fault Diagnosis in Induction Motors Through Torque Monitoring, IEEE Transactions on Energy Conversion, vol. 28, no. 2 (2013), pp. 267 - 277

[26] P.F. Albrecht, J.C. Appiarius, R.M. McCoy, E.L. Owen, D.K. Sharma Assessment of the Reliability of Motors in Utility Applications, IEEE Transactions on Energy Conversion, vol. EC-2, no. 3 (1987), pp. 39 - 46

[27] R.N. Bell, D.W. McWilliams, P. O'Donnell, C. Singh, S.J. Wells, (Motor Reliability Working Group) Report of Large Motor Reliability Survey of Industrial and Commercial Installations, Part I IEEE Transactions on Industry Applications, vol. IA-21, no. 4, (1985) pp. 853-864.

[28] P. Henrıquez, J.B. Alonso, M.A. Ferrer, C.M. Travieso Review of Automatic Fault Diagnosis System Using Audio and Vibration Signals, IEEE Transactions on Systems, Man, and Cybernetics: Systems, vol. 44, no. 5, (2014) pp. 642 - 652

[29] S.A. Mortazavizadeh, S.M.G. Mousavi A Review on Condition Monitoring and Diagnostic Techniques of Rotating Electrical Machines, Physical Science International Journal (2013)

[30] J. Guzinski, M. Diguet, Z. Krzemiński, A. Lewicki, H. Abu-Rub, Application of speed and load torque observers in high-speed train drive for diagnostic purposes, IEEE Transactions on Industrial Electronics, vol. 56, no 1 (2009)pp. 248-256.

[31] A. Balogun, O. Ojo, F. Okafor, S. Karugaba Determination of Steady-State and Dynamic Control Laws of Doubly Fed Induction Generator Using Natural and Power Variables IEEE Transactions on Industry Applications, VOL. 49, NO. 3 (2013), pp. 1343 - 1357

[32] Z. Krzeminski Nonlinear control of induction motor, in Proc. 10th World Congress on Automatic Control, IFAC (1987), Munich, Germany

[33] Z. Krzemiński Observer of induction motor speed based on exact disturbance model, in Proc. Int. Conf. EPE-PEMC Poznan, Poland. (2008)

[34] S. Mukherjee, G. Poddar (2007) Fast Control of Filter for Sensorless Vector Control SQIM Drive With Sinusoidal Motor Voltage, IEEE Transactions on Industrial Electronics, vol. 54, no. 5 (2007), pp. 2435-2442

[35] J. Guzinski, H. Abu-Rub, A. Iqbal, Sk. Moin Ahmed Shaft misalignment detection using ANFIS for speed sensorless ac drive with inverter output filter, IEEE International Symposium on Industrial Electronics ISIE 2011, Gdansk, Poland, pp. 2138 - 2143

[36] Sh. Hedayati Kia, H. Henao, G.-A. Capolino Torsional vibration monitoring using induction machine electromagnetic torque estimation, IECON (2008), pp. 3120 - 3125

[37] K. Ohishi, K. Nakano, I. Miyashita, S. Yasukawa Anti-slip control of electric motor coach based on disturbance observer, AMC'98 – Coimbra (1998),pp. 580 - 585

[38] Luigi Beneduce, Giovanni Caruso, Diego Iannuzzi, Franco Maceri , Enrico Pagano, Luigi Piegari Analysis of a structural failure mode arising in cage rotors of induction machines Electrical Engineering 93: (2011) pp.179–191

[39] Patryk Strankowski, Jaroslaw Guzinski „Detekcja uszkodzeń w bezczujnikowym napędzie elektrycznym z wykorzystaniem obserwatora momentu obciążenia", Maszyny Elektryczne – Zeszyty problemowe Nr. 107 Maj 2015

[40] Jaroslaw Guzinski, Patryk Strankowski „Detekcja uszkodzeń bezczujnikowego napędu elektrycznego z wykorzystaniem obserwatora momentu obciążenia", Napędy i sterowanie 05/2015

[41] P.J. TavnerReview of condition monitoring of rotating electrical machines, IET Electronics Power Applications, vol. 2, no 4 (2008), pp. 215-247

[42] A.C.J. Luo Past, current and future on nonlinear dynamics and noise origins of non-smooth gear transmission dynamic systems, Proc. IEEE Intelligent Vehicles SymposiumLas Vegas, USA. (2005)

[43] S. Prabhakar, A.S. Sekhar, A.R. Mohanty Crack versus coupling misalignment in a transient rotor system, Journal of Sound and Vibration, no. 256 (2002), pp. 773-786

[44] K. Szabat, T. Orlowska-Kowalska Performance Improvement of Industrial Drives with Mechanical Elasticity Using Nonlinear Adaptive Kalman Filter, IEEE Transactions on Industrial Electronics, vol. 55, no. 3 (2008), pp. 1075-1084.

[45] A. Dębowski, D. Lewandowski Application of the induction motor torque - observer to the control of turbo machines, EPE-PEMC (2008), Poznan, Poland, pp. 2320-2324

[46] B. Trajin, J. Regnier, J. Faucher Detection of bearing faults in asynchronous motors using Luenberger speed observer, 34th Annual Conference of IEEE Industrial Electronics Society, IECON 2008, 10-13 Nov. 2008, pp. 3073-3078

[47] A. Hace, K. Jezernik, A. Šabanovic SMC with disturbance observer for a linear belt drive, IEEE Transactions on Industrial Electronics, vol. 54, no. 6 (2007), pp. 3402-3412

[48] B. Gopinath On the Control of Linear Multiple Input-Output Systems, The Bell Technical Journal, vo1. 50, no. 3 (1971), pp. 1063-1081

[49] Krzemiński Z.: Nonlinear control of induction motor, 10th World Congress on Automatic Control, IFAC'87, 27–31 July 1987, Munich, Germany.

[50] Bogdan M. Wilamowski, J. Dawid Irwin Boca Raton The Industrial Electronics Handbook: Power Electronics and Motor Drives. CRC Press Taylor & Francis Group, 2011.